Tertiary lymphoid structures induced by CXCL13-producing CD4$^+$ T cells increase tumor infiltrating CD8$^+$ T cells and B cells in ovarian cancer

Masayo Ukita[1], Junzo Hamanishi[1], Hiroyuki Yoshitomi[2,3], Koji Yamanoi[1], Shiro Takamatsu[1], Akihiko Ueda[1], Haruka Suzuki[1], Yuko Hosoe[1], Yoko Furutake[1], Mana Taki[1], Kaoru Abiko[4], Ken Yamaguchi[1], Hidekatsu Nakai[5], Tsukasa Baba[6], Noriomi Matsumura[5], Akihiko Yoshizawa[7], Hideki Ueno[2,3], Masaki Mandai[1]

[1]Department of Gynecology and Obstetrics, Kyoto University Graduate School of Medicine, Kyoto, Japan
[2]Department of immunology, Kyoto University Graduate School of Medicine, Kyoto, Japan
[3]Institute for the Advanced Study of Human Biology (ASHBi), Kyoto University, Kyoto, Japan
[4]Department of Obstetrics and Gynecology, National Hospital Organization Kyoto Medical Center, Kyoto, Japan
[5]Department of Obstetrics and Gynecology, Kindai University Faculty of Medicine, Osaka, Japan
[6]Department of Obstetrics and Gynecology, Iwate Medical University, Iwate, Japan
[7]Department of Diagnostic Pathology, Kyoto University Graduate School of Medicine, Kyoto, Japan

Corresponding author
Junzo Hamanishi, MD, PhD.
Department of Gynecology and Obstetrics, Kyoto University Graduate School of Medicine, 54 Shogoin Kawaharacho, Sakyoku, Kyoto, Japan.
Tel.: +81-75-751-3269
E-mail: jnkhmns@kuhp.kyoto-u.ac.jp

Keywords Tertiary lymphoid structures, CXCL13, Tumor microenvironment, Ovarian cancer

Acknowledgement We thank all the members of the Center for Anatomical, Pathological and Forensic Medical Research and Medical Research Support Center, Graduate School of Medicine, Kyoto University for preparing microscope slides.

Contributors MU designed and performed the experiments, analyzed the data, and wrote the manuscript. JH and HY designed and directed the study and edited the manuscript. ST performed statistical analyses and commented on the manuscript. HN and KA provided the clinical data. YH assisted with the experiments. AU, HS, YF, MT, KYaman, KA, KYamag, TB, NM, AY, HU, and MM provided advice on the experiments and commented on the manuscript.

Funding This work was supported by a Grant-in-Aid for Scientific Research (B) (Grant Number

JP18H02945), Grant-in-Aid for JSPS Research Fellow (Grant Number JP19J12595), Grant-in-Aid for Challenging Exploratory Research (Grant Number JP20K20610), Grant-in-Aid for Research Activity Start-up (Grant Number JP20K22810), and Grant-in-Aid for Scientific Research (C) (Grant Number JP21K09541).

Ethics approval and consent to participate This study was approved by Kyoto University Graduate School and Faculty of Medicine, Ethics Committee (G531), Ethics Committee of Kindai University Faculty of Medicine (27-182), and Ethics committee of the National Hospital Organization Kyoto Medical Center (19-081). Informed consent was obtained in the form of opt-out on the Web site for the patients at Kyoto University and Kindai University. Written informed consent was obtained from the patients at Kyoto Medical Center. Animal experiments were approved by the Kyoto University Animal Research Committee. This study was conducted according to Declaration of Helsinki principles.

Competing interests None declared.

Date availability statement The data analyzed in this study were previously deposited in the Gene Expression Omnibus (GEO) at GSE39204 and GSE55512 by our laboratory. All data relevant to the study are included in the article or uploaded as supplementary information.

Abstract

Background: Tertiary lymphoid structures (TLSs) are transient ectopic lymphoid aggregates whose formation might be caused by chronic inflammation states, such as cancer. The presence of TLS is associated with a favorable prognosis in most solid malignancies. The recognition of the relevance of TLS to cancer has led to a growing interest in TLS as an immunomodulatory target to enhance tumor immunity, although how TLSs are induced in the tumor microenvironment (TME) and how they affect patient survival are not well understood.

Methods: TLS distribution in relation to tumor infiltrating lymphocytes (TILs) and related gene expression were investigated in high grade serous ovarian cancer (HGSC) specimens. CXCL13 expression, which is strongly associated with TLS, and its localization in immune cells, were examined. We explored the tumor microenvironment for CXCL13 secretion by adding various inflammatory cytokines *in vitro*. The induction of TLS by CXCL13 was examined in a mouse model of ovarian cancer.

Results: CXCL13 gene expression correlated with TLS formation and the infiltration of T cells and B cells, and was a favorable prognostic factor for HGSC patients. The coexistence of $CD8^+$ T cells and B-cell lineages in the TME was associated with a better prognosis of HGSC and was closely related to the presence of TLSs. CXCL13 expression was predominantly coincident with $CD4^+$ T cells in TLSs and $CD8^+$ T cells in TILs, and shifted from $CD4^+$ T cells to $CD21^+$ follicular dendritic cells as the TLS matured. Although TGF-β was reported to stimulate CXCL13 production, our *in vitro* results revealed

that CXCL13 secretion was promoted in $CD4^+$ T cells under TGF-β + IL-2-restricted conditions and in $CD8^+$ T cells under TGF-β + IL-12-rich conditions. In a mouse model of ovarian cancer, recombinant CXCL13 induced TLSs and enhanced survival by the infiltration of $CD8^+$ T cells.

Conclusions: TLS formation was promoted by CXCL13-producing $CD4^+$ T cells and TLSs facilitated the coordinated antitumor responses of cellular and humoral immunity in ovarian cancer.

Background

It is generally considered that the generation and regulation of an efficient adaptive immune response to cancer occurs in secondary lymphoid organs (SLOs) such as the regional lymph nodes. Antitumor immune cells are educated to recognize tumor antigens, proliferate in regional lymph nodes away from the tumor site, and then migrate into the tumor microenvironment (TME) to exert antitumor activity (1). Clinical studies have shown that higher densities of T cell subsets within the TME are associated with improved patient survival in several cancers including ovarian cancer (2-5). We previously reported that the forced infiltration of $CD8^+$ T cells into the TME by CCL19, a chemokine that attracts T cells, suppressed tumors in an ovarian cancer model (6). These results indicate that T cells have a critical role in the TME and that the TME might be a therapeutic target if effectively altered by immune-activating signals such as chemokines. To date, strategies to enhance the clinical efficacy of anti-tumor treatments have predominantly focused on the T cell component in the tumor, and the roles of other immune cell components have not been fully elucidated.

Recent studies have revealed an alternative immune response at the tumor site within SLO-like cellular aggregates called tertiary lymphoid structures (TLSs) (7). TLSs are transient ectopic lymphoid aggregates whose formation might be caused by chronic inflammation states, including autoimmune and infectious diseases, transplanted organ rejection, and cancer (7-9). The presence of TLS is associated with a favorable prognosis in most solid malignancies (10). Recently, it was reported that TLS-associated B cells synergized with T cells to contribute anti-tumor effects and that the presence of TLS and B cells in tumor sites enhanced the efficacy of immunotherapy (11-14). The recognition of the relevance of TLS to cancer has led to a growing interest in TLS as an immunomodulatory target to enhance tumor immunity, although how this can be induced therapeutically is not known.

The chemokines CXCL13, CCL19, and CCL21 are involved in lymphoid tissue-inducer (LTi) cell homing and lymph node development (8). Especially, CXCL13 was reported to be essential for the initial attraction of LTi cells and the formation of early lymph nodes (15). Although TLSs are thought to share the mechanisms of initial development with SLOs, TLS formation is distinct from the preprogrammed processes involved in SLOs and does not necessarily occur in all patients. The generation of TLS in inflamed tissues might be governed by specific inflammatory signals that have not been fully identified (7). In autoimmune diseases such as rheumatoid arthritis (RA), we showed that TGF-β and other proinflammatory cytokines enhanced CXCL13 production by $CD4^+$ T cells, and that CXCL13-producing $CD4^+$ T cells had an important role in the formation of TLS (16, 17). However,

whether the same mechanism can be applied to the case of malignant tumors including ovarian cancer has not been investigated.

In this study, we assessed the relationship between tumor infiltrating T or B cells subsets and the presence of TLS, and evaluated the prognostic impact of TLS in ovarian cancer. We also investigated whether CXCL13 promoted TLS formation and improved the prognosis of patients with ovarian cancer. The role of CXCL13-producing $CD4^+$ T cells in the generation of TLS was also investigated.

Methods

Human samples

Sixty-two and 35 high grade serous ovarian cancer (HGSC) patients who underwent primary surgery at Kyoto University Hospital from 1997 to 2015 and at Kindai University Hospital from 2009 to 2016, respectively, were enrolled. Their clinical characteristics are described in Supplemental Table S1. Patients who received chemotherapy or radiation therapy prior to surgery were excluded. Four other patients with typical TLSs who underwent initial surgery at the National Hospital Organization Kyoto Medical Center between 2017 and 2019 were also included in the study.

Immunohistochemical analysis and evaluation

Immunohistochemical (IHC) staining was performed using formalin-fixed, paraffin-embedded (FFPE) specimens obtained from the above patients by the streptavidin-biotin-peroxidase method as

previously described (4, 6). The samples were incubated with anti-CD8, anti-CD4, anti-CD20, anti-CD38, and anti-CD21 antibodies. The antibodies used are listed in Supplemental Table S2.

Two independent investigators trained in the pathology of ovarian cancer and blinded to the clinical data examined the H&E staining and IHC slides. TLSs were evaluated by H&E staining and CD20 positive cell aggregation as an indicator. Five sections at 400× magnification with the most abundant infiltration were manually counted and the mean count was calculated for $CD8^+$ T cells, $CD4^+$ T cells, and $CD20^+$ B cells. These immune cells in TLSs were not counted as tumor infiltrating lymphocytes (TILs). If their count was above the median, we defined them as CD8-high, CD4-high, and CD20-high tumor, respectively. Tumor infiltrated $CD38^+$ plasma cells were graded according to their intensity and fraction of positive cells as 0, 1, 2, or 3 (plasma cell score) according to previous reports (18,19). Cases with scores of 0 and 1 were defined as plasma cell-low tumor, and cases with scores of 2 and 3 were defined as plasma cell-high tumors.

Detection of CXCL13 mRNA by RNA ISH

We assessed CXCL13 by RNA in situ hybridization (ISH) (RNAscope® 2.5 HD Reagent kit (RED), Advanced Cell Diagnostics, Hayward, CA, USA). FFPE tissue sections were deparaffinized in xylene and subsequently dehydrated in an ethanol series. Tissue sections were incubated in target retrieval reagent at 100°C for 15 minutes, and then treated with protease at 40°C for 30 minutes. Hybridization with Hs-CXCL13 (for human) or Mm-Cxcl13 (for mouse) probes at 40°C for 2 hours, and the amplifier

and visualization (Fast RED) procedures were performed in accordance with the manufacturer's instructions. For multiplex detection using FFPE, an RNAscope® Fluorescent Multiplex Reagent kit v2 (Advanced Cell Diagnostics) was used. Double staining was performed for CXCL13 and CD8, CXCL13 and CD4, and CXCL13 and CD21(CR2). The target probes and reagents used were listed in Supplemental Table S2. CXCL13 was detected with Opal 690, and CD4, CD8, and CR2 with Opal 570. Fluorescence images were captured using a fluorescence microscope BZ-X800E (KEYENCE, Osaka, Japan), and the colocalization of CXCL13 with various immune cells was quantified using BZ-H4C/hybrid cell count software (KEYENCE).

HGSC gene expression analysis

HGSC specimens obtained from 28 patients who underwent primary surgery at Kyoto University Hospital from 1997 to 2012 were prepared for gene expression microarray analysis (KOV). The data were previously deposited in the Gene Expression Omnibus (Accession Numbers: GSE 39204 and GSE 55512).

The gene expression profile of the TCGA-OV RNA sequencing dataset (n=217) from The Cancer Genome Atlas (TCGA) Data Portal (http://cancergenome.nih.gov, illuminahiseq_rnaseqv2_Level_3_RSEM_genes_normalized_data files obtained and merged on 19, Oct, 2015) was used for survival analysis and correlation testing among CXCL13, TGF-β1, PDCD1, and CD274.

Gene expression and infiltrating immune cells analysis

Raw gene expression microarray data using Affymetrix HT_HG-U133A from TCGA ovarian serous cystadenocarcinoma samples were obtained from the GDC legacy archive (https://portal.gdc.cancer.gov/legacy-archive/) in the form of CEL files (n=522). Gene expression values were calculated by normalization using the RMA method with R package "affy" (http://www.R-project.org). Subsequently, the relative abundance of 22 immune cell types for each sample was estimated using CIBERSORT (http://cibersort.stanford.edu/).

T cell receptor (TCR) and B cell receptor (BCR) repertoire analysis

TLSs and tumor areas were identified by microscopy and macrodissected independently from FFPE sections (Supplemental Figure S1C). RNA was extracted using NucleoSpin® total RNA FFPE (Takara Bio, Shiga, Japan) according to the manufacturer's instructions. Sequencing of the TCRα (TRA) and BCR IgG heavy chain loci were performed at Repertoire Genesis Incorporation (Osaka, Japan) using an unbiased amplification method with MiSeq (Illumina, San Diego, CA, USA). Data processing, assignment, and aggregation were performed using a repertoire analysis software program, Repertoire Genesis (RG), provided by Repertoire Genesis Incorporation. RG assigns TRV and TRJ alleles to queries and then generates CDR3 sequences, finally aggregating their combination patterns.

Induction assay of CXCL13 in $CD4^+$ and $CD8^+$ T cells

PBMCs from healthy donors were collected using Lymphocyte Separation Solution 1.077 (Nacalai Tesque, Kyoto, Japan). Blood $CD8^+$ T cells were isolated with CD8 MicroBeads, human (Miltenyi Biotec, Bergisch Gladbach, NRW, Germany). Blood $CD4^+$ T cells were purified with a Naïve $CD4^+$ T cell isolation kit II, human (Miltenyi Biotec) through a magnetic column.

Human T cells were differentiated for 6–7 days in a humidified 5% CO_2 incubator at 37°C with IMDM (Thermo Fisher, Waltham, MA, USA) supplemented with 10% fetal bovine serum, 100 units/ml penicillin and streptomycin under stimulation with 5 μg/ml plate-bound CD3 monoclonal antibody (clone: OKT3, Thermo Fisher) and 10 μg/ml CD28 monoclonal antibody (clone: CD28.2, Thermo Fisher) in the presence of 10 ng/ml TGF-β1 (Cell Signaling Technology, Danvers, MA, USA) unless otherwise described. Human T cells were also cultured under conditions where 5 μg/ml neutralizing anti-IL-2 antibody (R&D Systems, Minneapolis, MN, USA) or 10 ng/ml IL-12 (PeproTech, Montreal, Quebec, Canada) was added.

Human T cells were cultured under CD3/CD28 stimulation using conditioned medium from the human serous ovarian cancer cell lines: OVCA420, OVCA433, and DK-09. OVCA420 and OVCA433 were kindly provided by Dr. Susan K. Murphy of Duke University. DK-09 is a cell line that we established from the ascites of a patient with recurrent ovarian cancer (see Supplemental Methods). To block the TGF-β signals, a TGF-β signal inhibitor, SB431542 (Stemgent, Beltsville, MD, USA) was added at 0.5 and 5 μM.

211

212 **Flow cytometry**

213 For intracellular staining, cells were cultured for 4 hours with 4 μM monensin (Sigma-Aldrich, Saint
214 Louis, MO, USA), fixed, and stained with eBioscience™ Intracellular Fixation & Permeabilization
215 Buffer Set (Thermo Fisher) and antibodies for intracellular molecules. Fixable Viability Dye eFluor
216 506 (Thermo Fisher) was used to exclude dead cells. To detect CXCL13, CXCR5 and PD-1, the
217 antibodies listed in supplemental table S2 were used. Data were acquired using MACS Quant Analyzer
218 10 (Miltenyi Biotec) and were analyzed with FlowJo 10.0 (FlowJo LLC, Ashland, OR, USA).

219

220 **ELISA**

221 The concentrations of CXCL13 and TGF-β1 in the supernatant were measured with the respective
222 kits listed in Supplemental Table S2.

223

224 **Cell lines and tumor models**

225 The OV2944-HM-1(HM-1) mouse ovarian cancer cell line was purchased from RIKEN BioResource
226 Center (Ibaraki, Japan) and cultured as described (20). Throughout the study, we used HM-1 cell lines
227 passaged fewer than 20 times, and regularly tested for mycoplasma contamination. Female B6C3F1
228 (C57BL6 × C3/He F1) mice and nude mice (BALB/C-nu: CAnN.Cg-*Foxn1*^{nu}/Crl) were purchased
229 from Charles River Japan (Yokohama, Japan), and were maintained under specific pathogen-free

conditions.

A total of 1×10^6 HM-1 cells were inoculated intraperitoneally into B6C3F1 mice. Mouse recombinant CXCL13 (R&D Systems) treatment was initiated one day after the tumor inoculation and administered intraperitoneally at 1 μg/mouse every other day for five times. Control mice received PBS intraperitoneally. Then, 10–12 days after inoculating the tumor, mice were euthanized with carbon dioxide and the formation of TLS in omental tumors was analyzed.

A total of 2.5×10^5 HM-1 cells were inoculated intraperitoneally into B6C3F1 and nude mice. Similarly, rCXCL13 (1 μg/mouse) and anti-PD-L1 antibody (200 μg/mouse) were intraperitoneally administered 5 times every other day starting from day 1 and day 3, respectively, after tumor implantation. Anti-PD-L1 antibody (clone 10F.9G2, Bio X Cell, Lebanon, NH, USA) and Rat IgG antibody (clone LFT-2, Bio X Cell) were used as negative controls.

IHC analysis of mouse tumors

Mouse tumor cryosections (6-μm-thick) were stained with anti-CD4, anti-CD8 (clone YTS169.4), anti-CD19, and anti-Ki-67 antibodies as previously described (21). The antibodies are listed in Supplemental Table S2. Mouse FFPE specimens were stained with anti-CD8 antibody (clone EPR20305).

Statistics

Results are shown as the mean ± SEM from at least three independent experiments unless otherwise stated. A *P* value of less than 0.05 was considered statistically significant. Significance was calculated using the 2-tailed Student's *t*-test, and correlation between groups was determined by Spearman's correlation test. The log-rank test was used for overall survival analysis unless otherwise described. All statistical analyses were performed using GraphPad Prism 7 (GraphPad software, San Diego, CA, USA). The Jonckheere-Terpstra test was performed using the "clinfun" packages in R.

Results

TLS is associated with intratumor infiltration by $CD8^+$ T cells and B-cell lineages and is closely related to a favorable prognosis

The prognostic significance of the respective infiltration of T cell and B cell subsets was investigated by the IHC analysis of initial surgical specimens of HGSC (n=97) (Supplemental Table S1). Patients with a higher infiltration of $CD8^+$ T cells, $CD20^+$ B cells, and $CD38^+$ plasma cells had significantly prolonged progression free survival than those with low numbers of infiltrating cells ($P<0.05$, each) (Figure 1A). In addition, there was a significant correlation between the infiltrated number of $CD8^+$ T cells and B-cell lineage cells (Figure 1B), and patients with a higher number of infiltrated $CD8^+$ T cells and B-cell lineages had the best prognosis (Figure 1C). The intratumoral infiltration of $CD8^+$ T cells or B-cell lineages alone did not contribute to the improved prognosis.

H&E and IHC staining evaluation of TLSs in the same samples (n=97) revealed that 61 patients

(62.9%) had TLSs (Supplemental Table S1, Supplemental Figure S1, A and B). In the cases with TLS, the number of infiltrating $CD8^+$ T cells, $CD4^+$ T cells, $CD20^+$ B cells, or $CD38^+$ plasma cells (plasma cell score) was significantly higher than in those without TLS (P<0.0001, each) (Figure 1D). Focusing on the pattern of tumor infiltrating lymphocytes and the presence of TLS, TLS were found in 94% of cases with a high infiltration of $CD8^+$ T cells and B-cell lineages (CD8 high-CD20 high: n=35, CD8 high-plasma cell high: n=32) (Figure 1E). The close relationship between TLS and the distribution of infiltrating $CD8^+$ T cell and B-cell lineages suggests that cellular and humoral immunity interact via the TLS in ovarian cancer.

Next, we performed TCR and BCR repertoire analysis using tumor sections from HGSC patients (n=3), separating TLS and TIL regions by macrodissection (Supplemental Figure S1C). In two of three cases, TCR repertoire analysis showed many clones distributed in the TIL, whereas oligoclonal amplification was observed in TLS. Furthermore, the clone with the highest amplification from TIL was consistent with the clone observed in TLS (Figure 1F), suggesting that antigen-specific T cells that proliferated in TLS might also infiltrate into the tumor as TIL.

Patients with TLS, which is closely associated with intratumoral infiltration of $CD8^+$ T cells and B-cell lineages and may mediate cellular and humoral immunity, had a significantly better prognosis than patients without TLS (Wilcoxon test P=0.0016, median overall survival [110 months vs 70 months]) (Figure 1G).

CXCL13 gene expression in tumors correlates with TLS formation, lymphocyte infiltration, and a favorable prognosis for ovarian cancer

The expression of CXCL13 analyzed by RNA ISH demonstrated CXCL13 was highly expressed in TLS (Figure 2A). In addition, there were cases in which immune cells in the tumor stroma also expressed high levels of CXCL13 (Supplemental Figure S2A). From the IHC of initial surgical specimens with our original microarray data (KOV: GSE39204/55512, n=28), the ratio of cases with TLS was significantly higher in those with high CXCL13 gene expression than in those with low CXCL13 gene expression in tumor specimens(P=0.046) (Figure 2B). Additionally, CXCL13 gene expression was significantly correlated with the numbers of several types of TILs such as $CD4^+$ and $CD8^+$ T cells, $CD20^+$ B cells and $CD38^+$ plasma cells (P<0.001, each) (Figure 2C, Supplemental Figure S2B).

To validate these data, we applied CIBERSORT to examine the distribution of infiltrating immune cells into tumor sites and CXCL13 gene expression using the RNA sequence data of ovarian cancer cases registered in TCGA. The infiltration of $CD8^+$ T cells had the strongest correlation with CXCL13 gene expression, and that of $CD4^+$ T cells, $CD20^+$ B cells, $CD38^+$ plasma cells and M1-macropahges also showed a strong correlation with CXCL13 gene expression, while that of M2-macrophages and mature dendritic cells were negatively correlated , and that of natural killer cells and regulatory T (Treg) cells were not correlated with CXCL13 gene expression (Figure 2, D and E, Supplemental Figure S2, C and D). These results suggest that CXCL13 gene expression strongly correlated with the

306 formation of TLS and the number of tumor-infiltrating T cells and B-cell lineages.

307 Next, we examined the impact of CXCL13 on the prognosis of HGSC and found that patients with
308 high CXCL13 gene expression had a significantly better prognosis in the KOV data and TCGA data
309 (P<0.05, each) (Figure 2F).

310

311 **CXCL13 produced by CD4$^+$ T cells is critical for TLS initiation**

312 To identify cells producing CXCL13 involved in TLS formation, we performed RNA ISH double
313 staining (CXCL13 and CD4$^+$ T cells, CXCL13 and CD8$^+$ T cells) using HGSC tumor specimens. In
314 the TLS region, CXCL13 was highly coexpressed with CD4$^+$ T cells, whereas CD8$^+$ T cells
315 predominantly expressed CXCL13 in the tumor and stromal regions (Figure 3, A and B).

316 HGSC tissues contain two types of TLSs: early TLS, in which lymphocytes aggregate diffusely and
317 CD21$^+$ cells are scarce, and follicle-formed TLS, which has the follicular morphology of SLO and
318 where CD21$^+$ follicular dendritic cells (FDCs) are distributed in a reticular pattern (Figure 4, A and B).
319 Therefore, we performed the double staining of CXCL13 and CD8$^+$ T cells, CXCL13 and CD4$^+$ T cells,
320 and CXCL13 and CD21$^+$ FDCs by RNA ISH for representative early TLS and follicle-formed TLS.
321 CXCL13 expression was highly consistent with CD4$^+$ cells in early TLSs, whereas few CD4$^+$ T cells
322 expressing CXCL13 were observed in follicle-formed TLSs and CXCL13 expression was highly
323 consistent with spindle-shaped CD21$^+$ FDCs (Figure 4C). These results indicate that CXCL13-
324 producing CD4$^+$ T cells are closely related to the early stage of TLS formation.

TGF-β promotes the production of CXCL13

To investigate which factors promote CXCL13 secretion from $CD4^+$ T cells and $CD8^+$ T cells, we analyzed two sets of gene expression data from ovarian cancer tissues. Using the TCGA RNA sequence data and our KOV microarray data, we found a significant correlation between CXCL13 and TGF-β1 gene expression ($P<0.05$) (Figure 5A). The analysis of naïve $CD4^+$ T cells and $CD8^+$ T cells isolated from the peripheral blood cells of a healthy donor and cultured with TGF-β showed that $CD4^+$ T cells predominantly secreted CXCL13 compared with $CD8^+$ T cells. A TGF-β signal inhibitor (SB431542) suppressed the secretion of CXCL13 in a concentration-dependent manner (Figure 5B).

We previously reported that the TGF-β signaling pathway was activated in ovarian cancer (22), and we detected high concentrations of TGF-β1 in the conditioned medium of three different human ovarian cancer cell lines (Figure 5C). Using these conditioned media, we examined their effects on CXCL13 production in naïve $CD4^+$ and $CD8^+$ T cells. In $CD4^+$ T cells, CXCL13 secretion was promoted in the order of TGF-β1 concentration, and was suppressed in a concentration-dependent manner when incubated with the TGF-β signal inhibitor (SB431542) (Figure 5D). However, TGF-β-mediated CXCL13 secretion in $CD8^+$ T cells was limited.

Next, we conducted similar experiments by adding various cytokines to TGF-β to reproduce the TME. We found that CXCL13 secretion was enhanced in $CD4^+$ T cells under IL-2-restricted conditions and in $CD8^+$ T cells under IL-12-enriched conditions (Figure 5E). The CXCL13 concentration in the

culture supernatant showed a similar trend (Figure 5F). CXCL13-producing $CD4^+$ cells had a PD-1 positive, CXCR5 negative phenotype (Figure 5G). These results suggest that the phase and TME in which $CD4^+$ and $CD8^+$ T cells produce CXCL13 are different, and thus $CD4^+$ T cells may produce CXCL13 in TLSs and $CD8^+$ T cells in TILs (Figure 3, A and B).

Mouse recombinant CXCL13 induces TLS in tumors and prolongs survival

The effect of CXCL13 on TLS formation in tumors was analyzed using a mouse ovarian cancer model. A mouse ovarian cancer cell line HM-1 was intraperitoneally inoculated to B6C3F1 immunocompetent mice, and mouse recombinant(r) CXCL13 was intraperitoneally administered 5 times every other day starting from day 1, and TLS formed in the omental tumor were evaluated on days 10–12. The area of TLSs per tumor area was significantly increased in the rCXCL13-treated group compared with the control group (Figure 6A). IHC revealed that mouse TLS, similar to human TLS, consisted mainly of $CD19^+$ B cells, and that $CD8^+$ T cells and $CD4^+$ T cells were present in and around TLSs. Furthermore, TLSs contained many Ki-67 positive immune cells indicating these structures were immunologically activated (Supplemental Figure S3A). Furthermore, CXCL13 was highly expressed and corresponding with TLSs (Figure 6B). The administration of rCXCL13 markedly increased the infiltration of $CD8^+$ T cells around the TLSs (Figure 6C).

Next, we observed the effect of rCXCL13 administration on the survival of mice. In immunocompetent mice (B6C3F1), the survival time was significantly prolonged in the rCXCL13-

363 treated group compared with the control group (Figure 6D). Because there was a correlation between
364 CXCL13 and PD-1/PD-L1 gene expression (Supplemental Figure S3B), we hypothesized that
365 CXCL13 had an adjuvant effect in HM-1 ovarian cancer models that were originally refractory to anti-
366 PD-1/PD-L1 antibody therapy. However, no significant prognostic improvement was observed
367 (Supplemental Figure S3C).
368 Furthermore, the administration of rCXCL13 to immunocompromised mice (nude mice) did not
369 improve survival (Figure 6E). Consistent with the apparent increase in $CD8^+$ T cells around the TLSs
370 in immunocompetent mice, CXCL13 contributed to their improved survival via immunity. These
371 results indicate that CXCL13 induced TLSs and TILs, indicating CXCL13 and TLS might be new
372 therapeutic targets for ovarian cancer.
373
374 **Discussion**
375 We showed that the presence of TLS was associated with an increased intratumor infiltration of $CD8^+$
376 T cells and B-cell lineages, and that $CD8^+$ T cells and B-cell lineages might cooperate to improve the
377 prognosis of ovarian cancer. It was reported that tumor infiltrating B cells contributed to tumor growth
378 and progression through the production of cytokines, such as IL-10, that inhibit antitumor immunity
379 although the functional role of B cells in cancer is poorly understood (23). Recently, there have been
380 increasing numbers of reports that the presence of B cells, especially those associated with TLSs, may
381 improve cancer outcomes (10, 12-14). Tumors containing $CD8^+$ T cells and B-cell lineages were

associated with improved prognosis in melanoma, sarcoma, and ovarian cancer (12, 13, 18). In this study, we found a strong correlation between the infiltrated numbers of $CD8^+$ T cells and B-cell lineages, and confirmed the presence of TLS in 94% of patients with tumors containing high numbers of infiltrated T and B cells. These results suggest that B-cell lineages are an essential component of the $CD8^+$ T cell cytotoxic reaction, and that cellular and humoral immune interactions are mediated by TLSs.

Whether tumor-associated TLSs are formed in response to a series of chronic inflammation or whether they are induced as a tumor antigen-specific immune response has not been fully established. De Chaisemartin et al. demonstrated that TLSs provided the specialized vasculature and chemoattractants necessary for T cell infiltration into non-small cell lung cancer (NSCLC) (24). The TCR repertoire analysis of NSCLC showed that the expansion of T cell clones in the tumor bed and peripheral blood correlated with the density of tumor associated TLSs (25). In this study, TCR repertoire analysis of the TLSs and tumor regions revealed that oligoclonal expansion occurred in TLS and that the same clone was highly amplified in the tumor. These data suggest that the recognition of antigens occurs in TLS and that the effector T cell clones amplified by the TLS infiltrate into tumors, both of which might provide evidence that TLS promotes immune responses in TME.

High CXCL13 gene expression was associated with disease activity and pathogenicity in autoimmune diseases such as RA (26-28), and with patients' prognosis in several types of cancer (7, 29, 30), implying the strong involvement of CXCL13-dependent TLS formation. In line with previous reports,

CXCL13 gene expression is a prognostic factor for ovarian cancer and is strongly associated with the formation of TLS. The presence of TLS also improved the long-term prognosis of ovarian cancer.

We previously reported that CXCL13-producing PD-1 high CXCR5 negative $CD4^+$ T cells have an important role in the function of TLS in RA (16, 17). Although FDCs are the main source of CXCL13 in SLOs (31), the origin of CXCL13 in tumor associated TLS depends on the type of cancer. CXCL13 was secreted by PD-1^{high} $CD8^+$ T cells in lung cancer (32), by $CD103^+$ $CD8^+$ cells in ovarian cancer (33), and by $CXCR5^-$ PD-1^{high} $CD4^+$ follicular helper like T cells in breast cancer (34). In this study, CXCL13 was predominantly expressed on $CD4^+$ T cells in TLSs and on $CD8^+$ and $CD4^+$ T cells in TILs, and that the expression of CXCL13 in TLSs shifted from $CD4^+$ T cells to $CD21^+$ FDCs. Sequential stages of the development in tumor-associated TLS were observed in lung cancer. Siliņa et al. defined three types of TLSs: early TLS (E-TLS) without FDCs or germinal centers (GC), primary follicle like TLS (PFL-TLS) with an FDC network and lacking GC, and secondary follicle like TLS (SFL-TLS) with an FDC network and GC formation (35). Our data suggest that CXCL13-producing $CD4^+$ T cells are an important primary producer of CXCL13 in the early stages of TLS when FDCs are not present. FDCs emerge from ubiquitous perivascular mesenchymal cells expressing platelet-derived growth factor receptor β (36). CXCL13 itself directly induces lymphotoxin (LT) production by naïve B cells, and this CXCL13/LT pathway is crucial for FDC differentiation (37-39). We consider that FDC becomes the main source of CXCL13 in TLSs after the FDC network is formed, similar to that in SLOs.

The CXCL13-producing PD-1 high CXCR5 negative $CD4^+$ T cells we reported in RA (16, 17) do not express CXCR5, a marker typical of follicular helper T cells (Tfh). In the current study, the $CD4^+$ T cells in which CXCL13 expression was induced were PD-1 high CXCR5 negative. The CXCL13-producing $CD4^+$ T cells reported in breast cancer (34) had similar characteristics. The comprehensive analysis of blood and synovial samples of RA patients was used to propose a pathogenic PD-1^{high} $CXCR5^-$ CD4 subset as peripheral helper T cells (Tph) (40, 41). Tph cells express factors that enable B-cell help, including IL-21, CXCL13, and ICOS. Similar to PD-1^{high}-$CXCR5^+$ Tfh, Tph cells induce plasma cell differentiation *in vitro* through IL-21 secretion and SLAMF5 interactions (40). In this context, CXCL13-producing $CD4^+$ T cells not only promote the initial formation of TLSs but may also support anti-tumor antibody responses by B cells. Evidence for this was shown in our study, where B-cell lineages were clearly increased in patients with TLS and were associated with an improved prognosis. However, further research related to the co-localization of antigen-specific B cells with Tph cells in TLSs is warranted at the molecular level.

Proinflammatory conditions involving TGF-β promoted the differentiation of CXCL13-producing $CD4^+$ T cells in our previous studies (16, 17) and in breast and ovarian cancers (33, 34). Resident fibroblasts and macrophages, and infiltrating Tregs produce TGF-β locally (42). Previously, we reported that the TGF-β signaling pathway was activated in advanced ovarian cancer and promoted tumor progression and metastasis (22). Indeed, high levels of TGF-β1 were detected in the conditioned medium of DK-09, a cell line we established from the ascites of a recurrent multidrug-resistant HGSC

patient. In this study, we performed a CXCL13 induction assay using PBMCs from a healthy donor and found that TGF-β promoted CXCL13 secretion, although there was a significant difference in response to TGF-β between $CD4^+$ T cells and $CD8^+$ T cells. Furthermore, CXCL13 production was enhanced in $CD4^+$ T cells under an IL-2 restricted environment and in $CD8^+$ T cells under an IL-12 rich environment.

In addition to TGF-β, IL-2 is involved in the differentiation of $CD4^+$ T cells. Quenching IL-2 by Treg or dendritic cells was reported to contribute to the differentiation of Tfh and Th17 cells (43, 44). In our previous studies, an IL-2 neutralizing antibody enhanced CXCL13 production by PD-1^{high} $CXCR5^-$ $CD4^+$ T cells in RA (16, 17). Gu-Trantien et al. reported that IL-2 deprivation was critical for the production of CXCL13 and the accumulation of activated Tregs in parallel with $CXCL13^+CD4^+$ TIL in breast cancer (34). However, IL-12 produced by dendritic cells and macrophages has an essential role in the interactions between the innate and adaptive immune systems. IL-12 promotes $CD8^+$ cytotoxic T cell activation and expansion (45-47). Our findings that the secretory environment of CXCL13 was different between $CD4^+$ and $CD8^+$ T cells is interesting and consistent with the different predominance of cells expressing CXCL13 between TLSs and TILs in ovarian cancer tumor sections. The environment of CXCL13 production differs between $CD4^+$ and $CD8^+$ T cells, and their roles in the formation and maintenance of TLSs may be different, and should be studied in future experiments.

Last, we evaluated whether TLS was induced by CXCL13. In a mouse model of spontaneously developing gastric cancer by activated STAT3 signaling, chemokines, CXCL13, CCL19, and CCL21

were induced simultaneously with tumorigenesis and TLS formation (48). We administered mouse rCXCL13 one day after tumor inoculation and succeeded in inducing TLSs. CXCL13 was highly expressed and corresponding with TLSs. CXCL13 signals B cells to enhance LT production (37, 49), and the exogenous CXCL13 may have promoted a positive feed-forward loop. In the CXCL13 treated group, the infiltration of $CD8^+$ T cells around the TLS was clearly increased, and the survival time of tumor-bearing mice was also prolonged. Direct antitumor effects by CXCL13 were also observed in a colon cancer model. However, tumor growth was accelerated in CXCR5 or Rag1 knockout mice (30). The CXCL13 axis is a functional part of the relevant immune control and the TME can be altered by inducing CXCL13 and TLSs. Accordingly, our results clearly demonstrate that the induction of CXCL13 and TLSs has potential as an immune-modulatory target for ovarian cancer.

Taken together, CXCL13 is a strong prognostic factor for ovarian cancer, and is highly involved in the formation of TLS. CXCL13-producing $CD4^+$ T cells induced by TGF-β under an IL-2 restricted tumor environment are important for the initial formation of TLS. The presence of TLS mobilizes various lymphocytes, and in particular, the simultaneous infiltration of B-cell lineages that are critical for the cytotoxic response of $CD8^+$ T cells in ovarian cancer. The strong interaction between humoral and cellular immunity in the antitumor response was revealed, and the possibility of TLS-mediated interactions was demonstrated. *In vivo* experiments revealed the TME can be altered by inducing CXCL13 and TLSs, which might be an important immunomodulatory method to enhance antitumor immunity.

References

1. Mellman I, Coukos G, and Dranoff G. Cancer immunotherapy comes of age. *Nature.* 2011;480(7378):480-9.

2. Zhang L, Conejo-Garcia JR, Katsaros D, Gimotty PA, Massobrio M, Regnani G, et al. Intratumoral T Cells, Recurrence, and Survival in Epithelial Ovarian Cancer. *N Engl J Med.* 2003;348(3):203-13.

3. Fridman WH, Zitvogel L, Sautès-Fridman C, and Kroemer G. The immune contexture in cancer prognosis and treatment. *Nat Rev Clin Oncol.* 2017;14(12):717-34.

4. Hamanishi J, Mandai M, Iwasaki M, Okazaki T, Tanaka Y, Yamaguchi K, et al. Programmed cell death 1 ligand 1 and tumor-infiltrating CD8+ T lymphocytes are prognostic factors of human ovarian cancer. *Proc Natl Acad Sci U S A.* 2007;104(9):3360-5.

5. Abiko K, Mandai M, Hamanishi J, Yoshioka Y, Matsumura N, Baba T, et al. PD-L1 on Tumor Cells Is Induced in Ascites and Promotes Peritoneal Dissemination of Ovarian Cancer through CTL Dysfunction. *Clin Cancer Res.* 2013;19(6):1363-74.

6. Hamanishi J, Mandai M, Matsumura N, Baba T, Yamaguchi K, Fujii S, et al. Activated Local Immunity by CCL19-Transduced Embryonic Endothelial Progenitor Cells Suppresses Metastasis of Murine Ovarian Cancer. *Stem Cells.* 2010;28(1):164–173.

7. Pitzalis C, Jones GW, Bombardieri M, and Jones SA. Ectopic lymphoid-like structures in

infection, cancer and autoimmunity. *Nat Rev Immunol.* 2014;14(7):447-62.

8. Aloisi F, and Pujol-Borrell R. Lymphoid neogenesis in chronic inflammatory diseases. *Nat Rev Immunol.* 2006;6(3):205-17.

9. Jing F, and Choi EY. Potential of Cells and Cytokines/Chemokines to Regulate Tertiary Lymphoid Structures in Human Diseases. *Immune Netw.* 2016;16(5):271-80.

10. Sautes-Fridman C, Petitprez F, Calderaro J, and Fridman WH. Tertiary lymphoid structures in the era of cancer immunotherapy. *Nat Rev Cancer.* 2019;19(6):307-25.

11. Bruno TC. New predictors for immunotherapy responses sharpen our view of the tumour microenvironment. *Nature.* 2020;577(7791):474-6.

12. Cabrita R, Lauss M, Sanna A, Donia M, Skaarup Larsen M, Mitra S, et al. Tertiary lymphoid structures improve immunotherapy and survival in melanoma. *Nature.* 2020;577(7791):561-5.

13. Petitprez F, de Reynies A, Keung EZ, Chen TW, Sun CM, Calderaro J, et al. B cells are associated with survival and immunotherapy response in sarcoma. *Nature.* 2020;577(7791):556-60.

14. Helmink BA, Reddy SM, Gao J, Zhang S, Basar R, Thakur R, et al. B cells and tertiary lymphoid structures promote immunotherapy response. *Nature.* 2020.

15. Van De Pavert SA, Olivier BJ, Goverse G, Vondenhoff MF, Greuter M, Beke P, et al. Chemokine CXCL13 is essential for lymph node initiation and is induced by retinoic acid and neuronal stimulation. *Nat Immunol.* 2009;10(11):1193-9.

16. Kobayashi S, Watanabe T, Suzuki R, Furu M, Ito H, Ito J, et al. TGF-beta induces the differentiation of human CXCL13-producing CD4(+) T cells. *Eur J Immunol.* 2016;46(2):360-71.

17. Yoshitomi H, Kobayashi S, Miyagawa-Hayashino A, Okahata A, Doi K, Nishitani K, et al. Human Sox4 facilitates the development of CXCL13-producing helper T cells in inflammatory environments. *Nat Commun.* 2018;9(1):3762.

18. Kroeger DR, Milne K, and Nelson BH. Tumor-Infiltrating Plasma Cells Are Associated with Tertiary Lymphoid Structures, Cytolytic T-Cell Responses, and Superior Prognosis in Ovarian Cancer. *Clin Cancer Res.* 2016;22(12):3005-15.

19. Lohr M, Edlund K, Botling J, Hammad S, Hellwig B, Othman A, et al. The prognostic relevance of tumour-infiltrating plasma cells and immunoglobulin kappa C indicates an important role of the humoral immune response in non-small cell lung cancer. *Cancer Lett.* 2013;333(2):222-8.

20. Peng J, Hamanishi J, Matsumura N, Abiko K, Murat K, Baba T, et al. Chemotherapy Induces Programmed Cell Death-Ligand 1 Overexpression via the Nuclear Factor-κB to Foster an Immunosuppressive Tumor Microenvironment in Ovarian Cancer. *Cancer Res.* 2015;75(23):5034-45.

21. Horikawa N, Abiko K, Matsumura N, Hamanishi J, Baba T, Yamaguchi K, et al. Expression of Vascular Endothelial Growth Factor in Ovarian Cancer Inhibits Tumor Immunity through

the Accumulation of Myeloid-Derived Suppressor Cells. *Clin Cancer Res.* 2017;23(2):587-99.

22. Yamamura S, Matsumura N, Mandai M, Huang Z, Oura T, Baba T, et al. The activated transforming growth factor-beta signaling pathway in peritoneal metastases is a potential therapeutic target in ovarian cancer. *Int J Cancer.* 2012;130(1):20-8.

23. Yuen GJ, Demissie E, and Pillai S. B Lymphocytes and Cancer: A Love–Hate Relationship. *Trends Cancer.* 2016;2(12):747-57.

24. De Chaisemartin L, Goc J, Damotte D, Validire P, Magdeleinat P, Alifano M, et al. Characterization of Chemokines and Adhesion Molecules Associated with T cell Presence in Tertiary Lymphoid Structures in Human Lung Cancer. *Cancer Res.* 2011;71(20):6391-9.

25. Zhu W, Germain C, Liu Z, Sebastian Y, Devi P, Knockaert S, et al. A high density of tertiary lymphoid structure B cells in lung tumors is associated with increased CD4+T cell receptor repertoire clonality. *OncoImmunology.* 2015;4(12):e1051922.

26. Takemura S, Braun A, Crowson C, Kurtin PJ, Cofield RH, O'Fallon WM, et al. Lymphoid Neogenesis in Rheumatoid Synovitis. *J Immunol.* 2001;167(2):1072-80.

27. Shi K, Hayashida K, Kaneko M, Hashimoto J, Tomita T, Lipsky PE, et al. Lymphoid Chemokine B Cell-Attracting Chemokine-1 (CXCL13) Is Expressed in Germinal Center of Ectopic Lymphoid Follicles Within the Synovium of Chronic Arthritis Patients. *J Immunol.* 2001;166(1):650-5.

28. Wutte N, Kovacs G, Berghold A, Reiter H, Aberer W, and Aberer E. CXCL13 and B-cell

activating factor as putative biomarkers in systemic sclerosis. *Br J Dermatol.* 2013;169(3):723-5.

29. Gu-Trantien C, Loi S, Garaud S, Equeter C, Libin M, de Wind A, et al. CD4(+) follicular helper T cell infiltration predicts breast cancer survival. *J Clin Invest.* 2013;123(7):2873-92.

30. Bindea G, Mlecnik B, Tosolini M, Kirilovsky A, Waldner M, Anna, et al. Spatiotemporal Dynamics of Intratumoral Immune Cells Reveal the Immune Landscape in Human Cancer. *Immunity.* 2013;39(4):782-95.

31. Gunn MD, Ngo VN, Ansel KM, Ekland EH, Cyster JG, and Williams LT. A B-cell-homing chemokine made in lymphoid follicles activates Burkitt's lymphoma receptor-1. *Nature.* 1998;391(6669):799-803.

32. Thommen DS, Koelzer VH, Herzig P, Roller A, Trefny M, Dimeloe S, et al. A transcriptionally and functionally distinct PD-1+ CD8+ T cell pool with predictive potential in non-small-cell lung cancer treated with PD-1 blockade. *Nat Med.* 2018;24(7):994-1004.

33. Workel HH, Lubbers JM, Arnold R, Prins TM, Van Der Vlies P, De Lange K, et al. A Transcriptionally Distinct CXCL13+CD103+CD8+ T-cell Population Is Associated with B-cell Recruitment and Neoantigen Load in Human Cancer. *Cancer Immunol Res.* 2019;7(5):784-96.

34. Gu-Trantien C, Migliori E, Buisseret L, De Wind A, Brohée S, Garaud S, et al. CXCL13-producing TFH cells link immune suppression and adaptive memory in human breast cancer.

572 *JCI Insight.* 2017;2(11).

573 35. Siliņa K, Soltermann A, Attar FM, Casanova R, Uckeley ZM, Thut H, et al. Germinal Centers
574 Determine the Prognostic Relevance of Tertiary Lymphoid Structures and Are Impaired by
575 Corticosteroids in Lung Squamous Cell Carcinoma. *Cancer Res.* 2018;78(5):1308-20.

576 36. Krautler NJ, Kana V, Kranich J, Tian Y, Perera D, Lemm D, et al. Follicular Dendritic Cells
577 Emerge from Ubiquitous Perivascular Precursors. *Cell.* 2012;150(1):194-206.

578 37. Aguzzi A, Kranich J, and Krautler NJ. Follicular dendritic cells: origin, phenotype, and
579 function in health and disease. *Trends Immunol.* 2014;35(3):105-13.

580 38. Allen CDC, and Cyster JG. Follicular dendritic cell networks of primary follicles and germinal
581 centers: Phenotype and function. *Semin Immunol.* 2008;20(1):14-25.

582 39. Fleige H, Ravens S, Moschovakis GL, Bölter J, Willenzon S, Sutter G, et al. IL-17–induced
583 CXCL12 recruits B cells and induces follicle formation in BALT in the absence of
584 differentiated FDCs. *J Exp Med.* 2014;211(4):643-51.

585 40. Rao DA, Gurish MF, Marshall JL, Slowikowski K, Fonseka CY, Liu Y, et al. Pathologically
586 expanded peripheral T helper cell subset drives B cells in rheumatoid arthritis. *Nature.*
587 2017;542(7639):110-4.

588 41. Yoshitomi H. CXCL13-producing PD-1hiCXCR5− helper T cells in chronic inflammation.
589 *Immunol Med.* 2020;43(4):156-60.

590 42. Huang M, Sharma S, Zhu LX, Keane MP, Luo J, Zhang L, et al. IL-7 inhibits fibroblast TGF-

β production and signaling in pulmonary fibrosis. *J Clin Invest.* 2002;109(7):931–937.

43. Liu Z, Gerner MY, Van Panhuys N, Levine AG, Rudensky AY, and Germain RN. Immune homeostasis enforced by co-localized effector and regulatory T cells. *Nature.* 2015;528(7581):225-30.

44. Li J, Lu E, Yi T, and Cyster JG. EBI2 augments Tfh cell fate by promoting interaction with IL-2-quenching dendritic cells. *Nature.* 2016;533(7601):110-4.

45. Teng MW, Bowman EP, McElwee JJ, Smyth MJ, Casanova JL, Cooper AM, et al. IL-12 and IL-23 cytokines: from discovery to targeted therapies for immune-mediated inflammatory diseases. *Nat Med.* 2015;21(7):719-29.

46. Colombo MP, and Trinchieri G. Interleukin-12 in anti-tumor immunity and immunotherapy. *Cytokine Growth Factor Rev.* 2002;13(2):155-68.

47. Lin L, Rayman P, Pavicic PG, Tannenbaum C, Hamilton T, Montero A, et al. Ex vivo conditioning with IL-12 protects tumor-infiltrating CD8+ T cells from negative regulation by local IFN-γ. *Cancer Immunol Immunother*. 2019;68(3):395-405.

48. Hill DG, Yu L, Gao H, Balic JJ, West A, Oshima H, et al. Hyperactive gp130/STAT3-driven gastric tumourigenesis promotes submucosal tertiary lymphoid structure development. *Int J Cancer*. 2018;143(1):167-78.

49. Aguzzi A, and Krautler NJ. Characterizing follicular dendritic cells: A progress report. *Eur J Immunol*. 2010;40(8):2134-8.

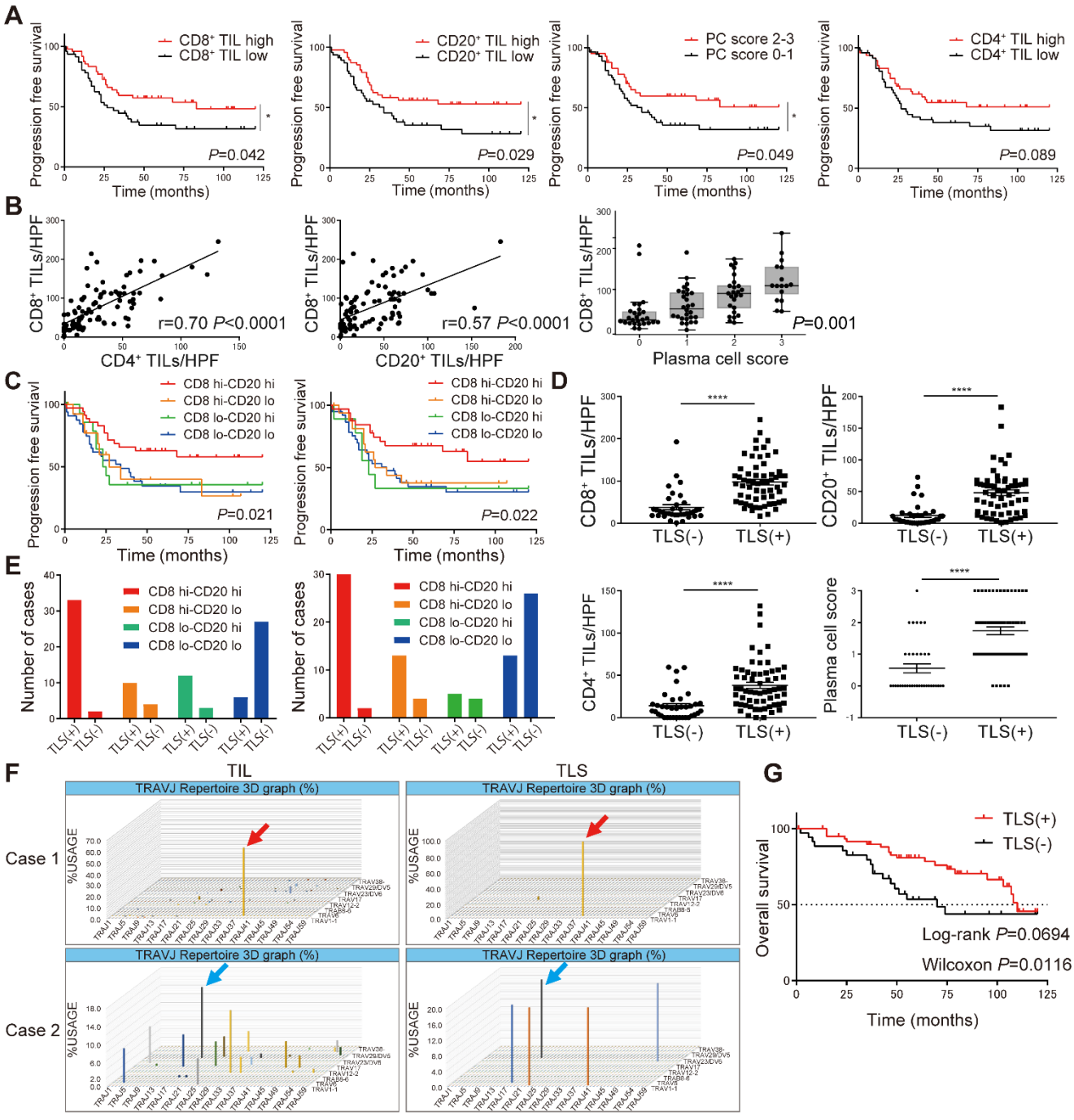

Figure 1. TLS is associated with intratumor infiltration by CD8⁺ T cells and B-cell lineages and is closely related to a favorable prognosis. (A) Progression free survival of the cohort stratified by CD8⁺ T cells, CD20⁺ B cells, plasma cells (PC), and CD4⁺ T cells (n=97, each). **(B)** Association between infiltrated numbers of CD4⁺ T cells and CD8⁺ T cells, and CD8⁺ T cells and B cell lineages in tumors (n=97). Correlations were determined by Pearson's correlation test and Jonckheere-Terpstra trend tests. **(C)** Progression free survival of patients based on the tumor-infiltrating CD8⁺ T cells and B lineage cells (CD8 hi-CD20 hi: n=35, CD8 hi-CD20 lo: n=14, CD8 lo-CD20 hi: n=15, CD8 lo-CD20 lo: n=33, total n=97) (CD8 hi-PC hi: n=32, CD8 hi-PC lo: n=17, CD8 lo-PC hi: n=9, CD8 lo-PC lo: n=39, total n=97). **(D)** The number of tumor-infiltrating CD8⁺ T cells, CD20⁺ B cells, plasma cells, and CD4⁺ T cells according to TLS presence (TLS− n=36, TLS+ n=61). *P* values were determined by Mann-Whitney *U*-test. **(E)**

Distribution of TLS in relation to the infiltration pattern of immune cells in tumors. Tumors were considered high (hi) for $CD8^+$ T cells, $CD20^+$ B cells and $CD4^+$ T cells if their score was above the median. Tumors were divided into two groups for PC by plasma cell score (0–1 n=56, 2–3 n=41), with 0–1 defined as PC low (lo) and 2–3 as PC hi in (A), (C), and (E). **(F)** TCR repertoire analysis separating TLS and TIL regions. The horizontal axis shows the J gene, the depth shows the V gene, and the vertical axis shows the frequency of usage. Clones indicated by arrows of the same color confirm the same amino acid sequence of CDR3. **(G)** Overall survival of patients with HGSC by the presence of TLS (TLS− n=36, TLS+ n=61, total n=97). Analyses were performed with Kaplan-Meier estimates and log-rank tests in (A) (C), and Wilcoxon tests (G).

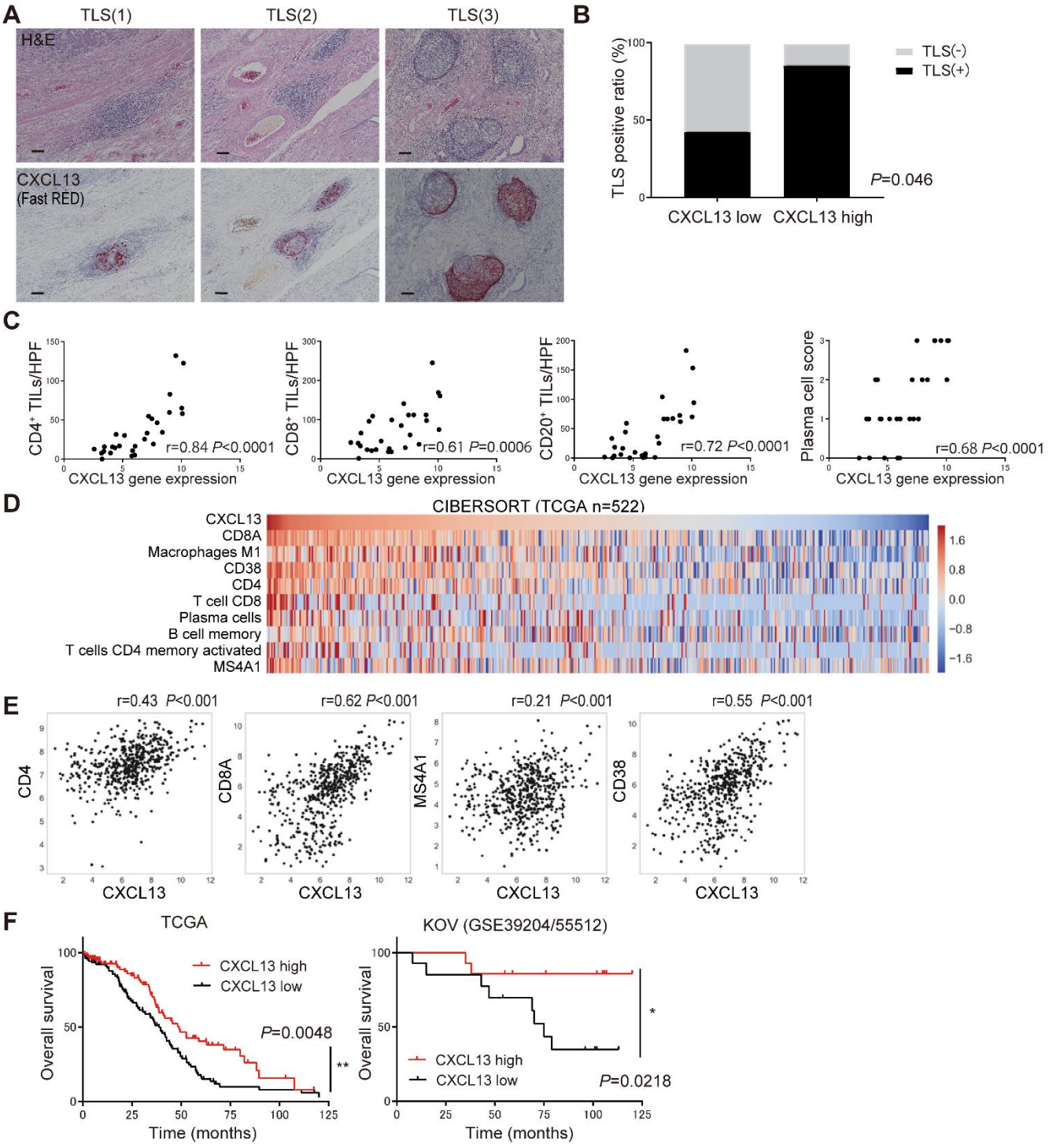

Figure 2. CXCL13 gene expression in tumors correlates with TLS formation, lymphocyte infiltration, and a favorable prognosis for ovarian cancer. (A) Representative TLS in tissues stained by H&E and CXCL13 (Fast RED) by RNA ISH. Scale bars indicate 100 µm. **(B)** TLS presence ratio based on CXCL13 gene expression. Analysis by Fisher's exact test in 28 cases with microarray data. **(C)** Characterization of the immune infiltrate in tumors according to CXCL13 gene expression (n=28). Correlation was determined by Spearman's correlation test. **(D) (E)** The distribution of infiltrating immune cells into the tumor site and CXCL13 gene expression using CIBERSORT (n=522). Correlation was determined by Spearman's correlation test. **(F)** Overall survival of patients with HGSC by

637 CXCL13 gene expression (TCGA n=217, KOV n=28). Patients with CXCL13 high defined if CXCL13 gene
638 expression was above the median. Analyses were performed with Kaplan-Meier estimates, log-rank tests and
639 Wilcoxon tests. The level of significance was set as *P<0.05, **P<0.01, and ****P<0.0001.
640

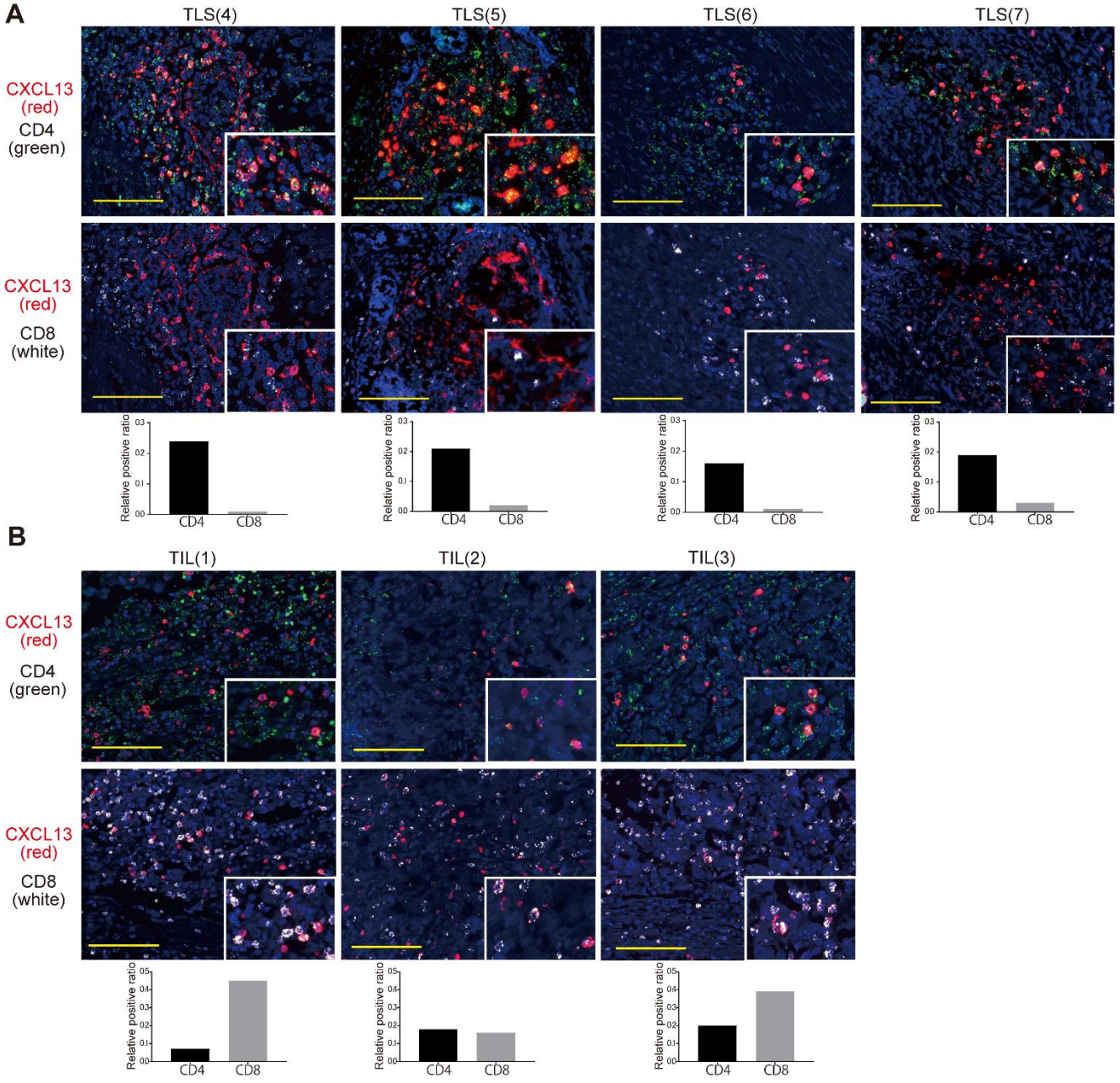

Figure 3. CXCL13 is mainly produced by CD4$^+$ T cells in TLS. (A) Fluorescent double staining of CXCL13 (red) and CD4 (green), and CXCL13 (red) and CD8 (white) by RNA ISH in TLS. Images of four representative TLS are shown. **(B)** Fluorescent double staining of CXCL13 (red) and CD4 (green), and CXCL13 (red) and CD8 (white) by RNA ISH in TIL. The upper and lower pictures are representative TIL images from the same patient. Nuclei are stained with DAPI (blue). Scale bars indicate 100 μm. Co-localization of CXCL13 with CD4 or CD8 is shown in the bar graph as the relative positive ratio quantified using BZ-H4C/hybrid cell count software.

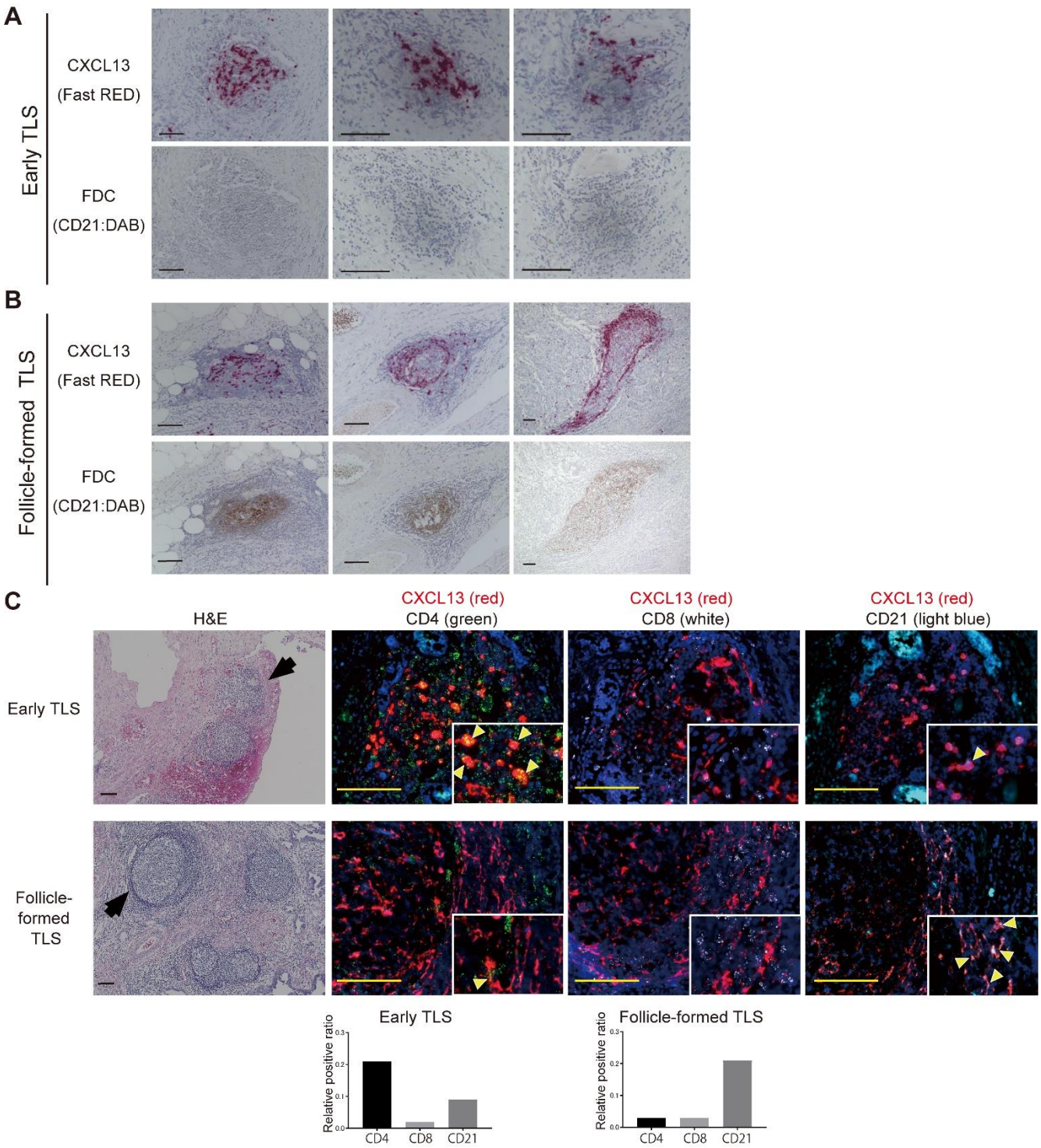

Figure 4. The source of CXCL13 production in TLS shifts to CD21$^+$ FDC with the maturation of TLS. (A) Representative images of early TLS. **(B)** Representative images of follicle-formed TLS. Upper panels show CXCL13 (RNA ISH, Fast RED) and lower panels show FDC (CD21 IHC, DAB). **(C)** Fluorescence double staining of CXCL13 (red) and CD4 (green), CXCL13 (red) and CD8 (white), and CXCL13 (red) and CD21 (light blue) in representative early TLS and follicle-formed TLS. Nuclei are stained with DAPI (blue). Scale bar indicates 100 μm. Co-localization of CXCL13 with CD4, CD8, or CD21 is shown in the bar graph as the relative positive ratio quantified using BZ-H4C/hybrid cell count software.

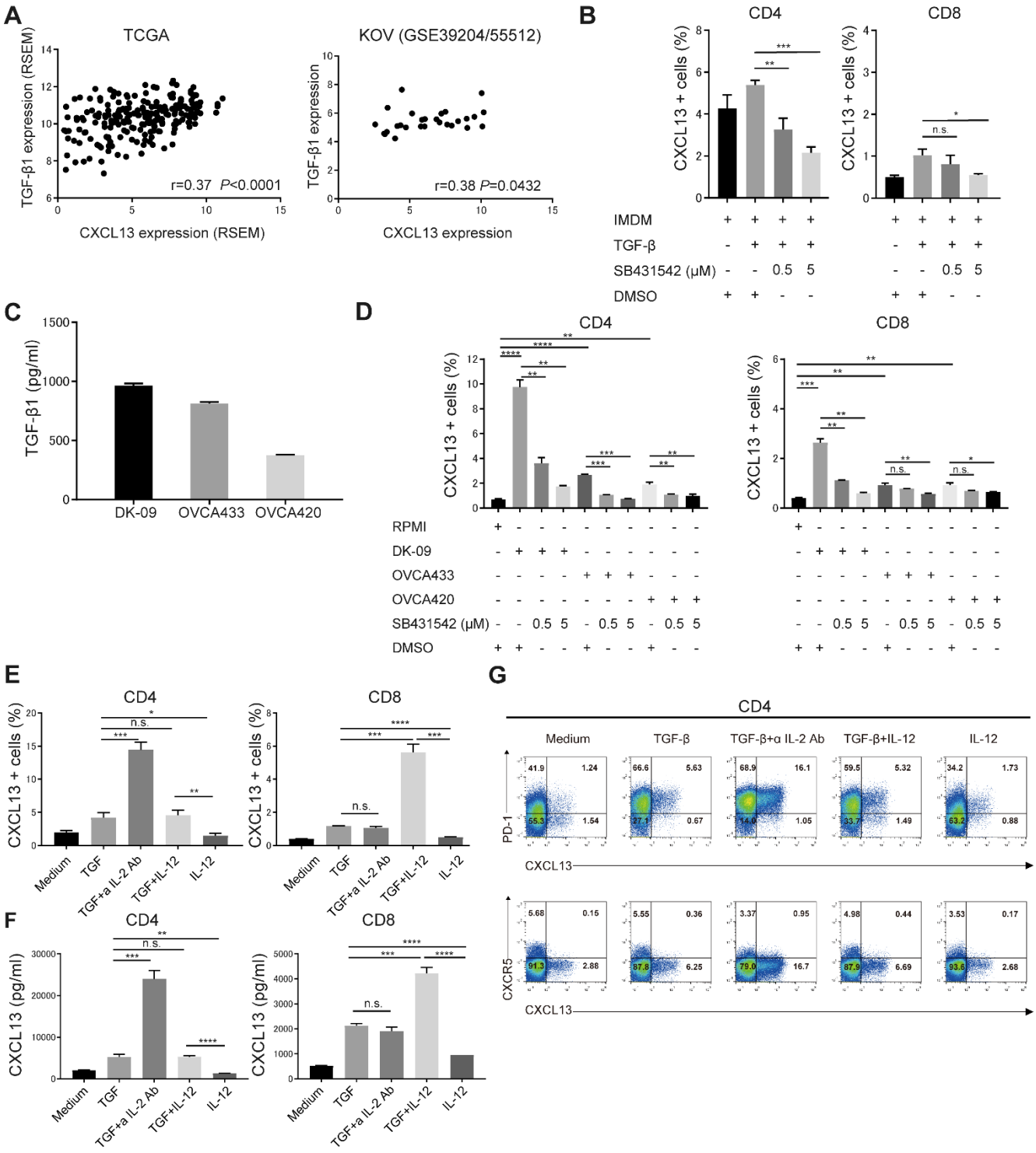

Figure 5. TGF-β promotes the production of CXCL13. (A) Correlation between CXCL13 and TGF-β1 expression in TCGA (n=217) and KOV (n=28). Correlation was determined by Spearman's correlation test. **(B)** Human naïve $CD4^+$ and $CD8^+$ T cells from a healthy donor were differentiated by TCR stimulation and TGF-β1 in the presence or absence of a TGF signal inhibitor, SB431542. The proportion of $CXCL13^+$ cells was determined by flow cytometry. Data are shown as the mean ± SEM of four samples. Statistical significance was determined by two-tailed Student's *t*-test, **P*<0.05, ***P*<0.01, ****P*<0.001, n.s.: not significant. **(C)** The concentration of TGF-β1 in conditioned medium obtained from three human ovarian cancer cell lines was measured by ELISA. Data are shown as the mean

± SEM of three samples. **(D)** Human naïve $CD4^+$ and $CD8^+$ T cells from a healthy donor were differentiated with TCR stimulation and conditioned medium obtained from three human ovarian cancer cell lines in the presence or absence of a TGF signal inhibitor, SB431542. The proportion of $CXCL13^+$ cells was determined by flow cytometry. Data are shown as the mean ± SEM of triplicates. **(E) (F) (G)** Human naïve $CD4^+$ and $CD8^+$ T cells from a healthy donor were differentiated with TCR stimulation and the indicated cytokines. The proportion of $CXCL13^+$ cells was determined by flow cytometry **(E)**. The concentration of CXCL13 in the culture supernatant was measured by ELISA **(F)**. Data are shown as the mean ± SEM of four samples in CD4 and three samples in CD8. Statistical significance was determined by two-tailed Student's *t*-test, $*P<0.05$, $**P< 0.01$, $***P < 0.001$, $****P<0.0001$, n.s.: not significant. Representative dot plots of PD-1 (upper row), CXCR5 (lower row), and intracellular CXCL13 in healthy human naïve $CD4^+$ T cells are shown **(G)**. a IL-2 Ab indicates anti IL-2 antibody.

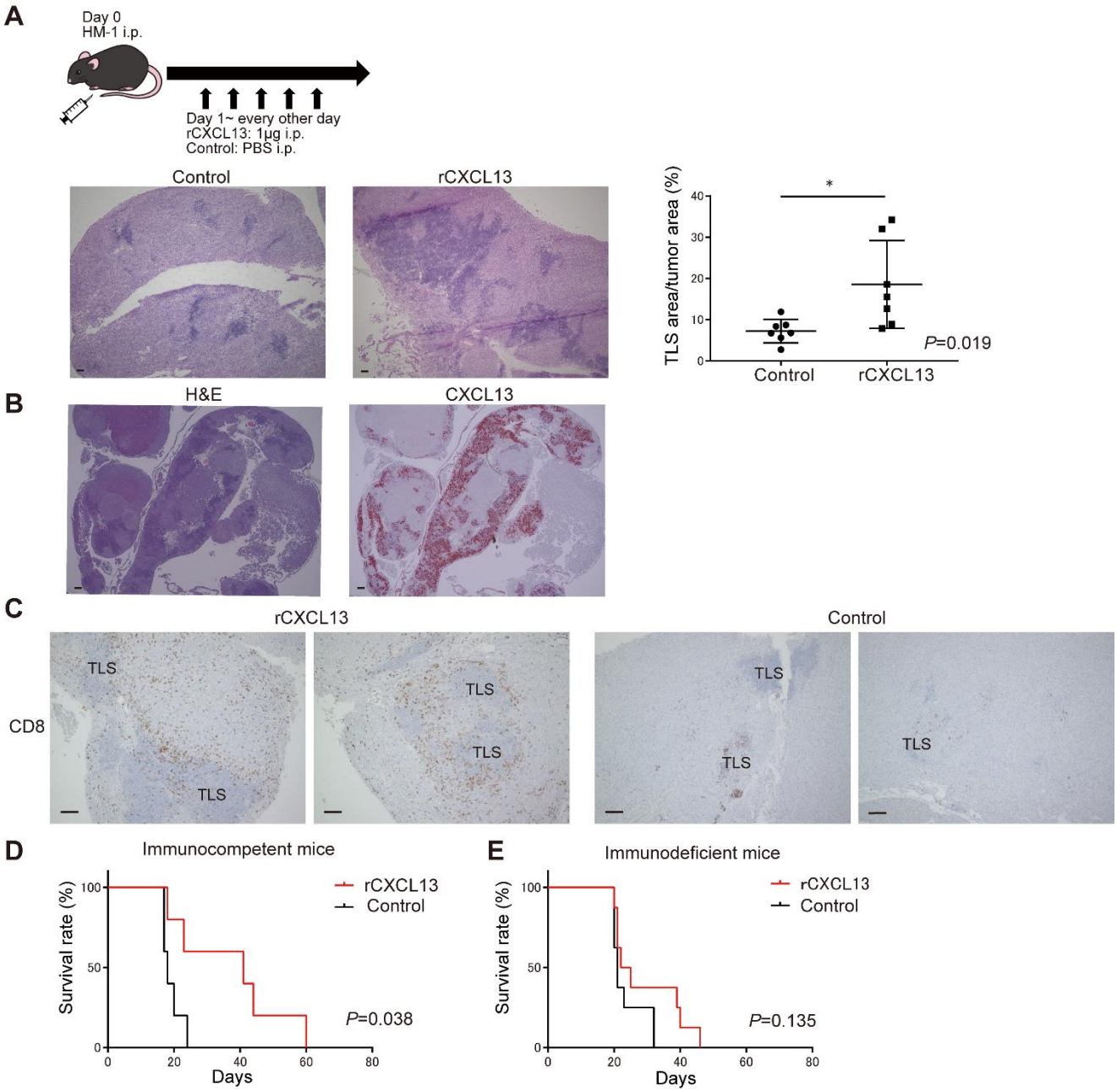

677

678 **Figure 6. Mouse recombinant CXCL13 induces TLS in tumors and prolongs survival. (A)** Mouse rCXCL13 was
679 administered intraperitoneally to induce TLS in a mouse ovarian cancer model. Representative H&E images of TLS
680 formed in an omental tumor. The area of TLS per tumor area was compared between the control group and the
681 rCXCL13 treated group (n=7, each). Statistical significance was determined by two-tailed Student's *t*-test, **P*<0.05.
682 **(B)** TLS induced by mouse rCXCL13 (H&E) and expression of mouse CXCL13 corresponding to TLS (RNA ISH,
683 Fast RED). **(C)** $CD8^+$ T cell IHC images (DAB) in the rCXCL13 treated group and control group. Scale bars indicate
684 100 μm. **(D) (E)** The effect of rCXCL13 administration on the survival of tumor-bearing mice was compared between
685 immunocompetent mice (D) and immunodeficient mice (E). Analyses were performed using Kaplan-Meier estimates
686 and log-rank tests.